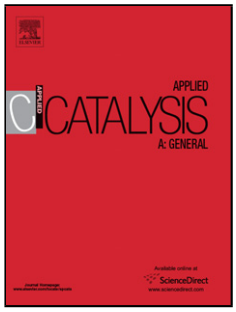

Title: Acid catalysis dominated suppression of xylose hydrogenation with increasing yield of 1,2-pentanediol in the acid-metal dual catalyst system

Authors: Nailiang Wang, Zhipeng Chen, Licheng Liu

PII: S0926-860X(18)30241-2
DOI: https://doi.org/10.1016/j.apcata.2018.05.019
Reference: APCATA 16668

To appear in: *Applied Catalysis A: General*

Received date: 6-3-2018
Revised date: 14-5-2018
Accepted date: 19-5-2018

Please cite this article as: Wang N, Chen Z, Liu L, Acid catalysis dominated suppression of xylose hydrogenation with increasing yield of 1,2-pentanediol in the acid-metal dual catalyst system, *Applied Catalysis A, General* (2018), https://doi.org/10.1016/j.apcata.2018.05.019

Acid catalysis dominated suppression of xylose hydrogenation with increasing yield of 1,2-pentanediol in the acid-metal dual catalyst system

Nailiang Wang[a], Zhipeng Chen[a,b], and Licheng Liu[a,*]

[a] CAS Key Laboratory of Bio-based Materials, Qingdao Institute of Bioenergy and Bioprocess Technology, Chinese Academy of Sciences, Songling Road 189, Qingdao 266101, China

[b] Graduate University of Chinese Academy of Sciences, Beijing 100049, P.R. China

[*]**Corresponding Author**

Licheng Liu

Tel.: +86-532-80662780

E-mail:liulc@qibebt.ac.cn

Graphical Abstract:

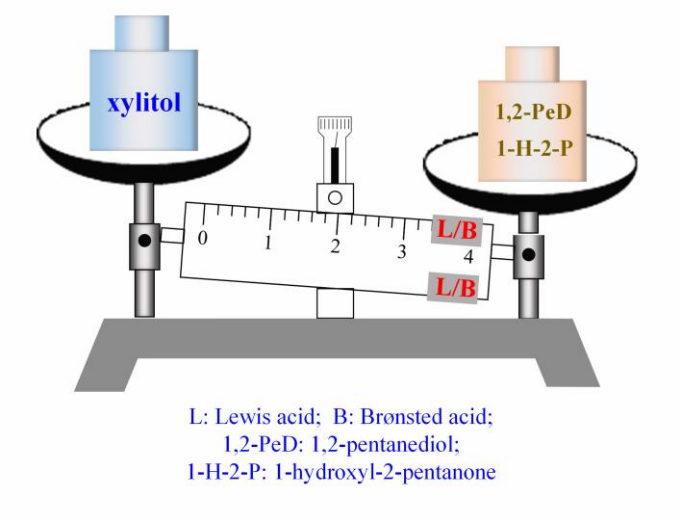

Highlights:

- Biphasic system assembly with two catalysts is built for the production of 1,2-PeD.
- Lewis acid site enhances the combined selectivity to 1,2-PeD ant its precursor.
- The lower E_a of xylose dehydration accounts for selectivity improvement.

Abstract

One-pot conversion of xylose to 1,2-pentanediol was investigated in a dual catalyst system composed of Ru/C and niobium phosphate as hydrogenation and acid catalysts, respectively. A series of niobium phosphate catalysts well-characterized by XRD, N_2 physisorption, FT-IR, NH_3-TPD, Py-IR and XPS were tested regarding the effect of their acid properties on product selectivity for the studied process. A systematic study was reported on the effect of reaction conditions. The combined yield of 21-27% to 1,2-pentanediol and its precursor 1-hydroxyl-2-pentanone was accomplished at

423 K under 3.0 Mpa hydrogen pressure in water-γ-valerolactone/cyclohexane biphasic system. At optimized conditions, the correlation between the product yield and the surface Lewis/Brønsted ratio were analyzed. The results revealed that the lower apparent activation energy of xylose dehydration reaction catalyzed by Lewis acid site accounted for the high product selectivity for sugar intermediate and furfural hydrogenation processes, especially for the combined selectivity to 1,2-pentanediol and 1-hydroxyl-2-pentanone. This study lays the grounds for further design of improved solid acid catalysts with high selectivity of 1, 2-pentanediol.

Keyword: Acid catalysis; 1,2-Pentanediol; One-pot conversion; Xylose; Xylitol

1. Introduction

1,2-Pentanediol (1,2-PeD) is a high-value chemical used as intermediate in the synthesis of cosmetics and chemicals [1, 2], especially for propiconazole [3]. Currently, various industrial processes relying on petroleum resources are available for the production of 1,2-PeD, an example being the oxidation of 1-pentene to 1,2-epoxypentene and subsequent hydrolysis to afford 1,2-PeD [4]. However, due to the use of high-polluting oxidants such as sodium hypochlorite and peracetic acid, increasingly serious environmental issues urge people to explore and utilize eco-friendly alternatives. The lignocellulosic material as a potential C_5 resource for the synthesis of 1,2-PeD has attracted significant attention worldwide in the past from the viewpoint of atom economy and sustainable development [5-8]. Using renewable xylose from hemicellulose to synthesize 1,2-PeD can reduce the environmental pressure owing to the absence of oxidant since oxygen elements are largely reserved in 1,2-PeD.

The multistep processes with furfural derivatives as reaction intermediate are mainly used to produce 1,2-PeD from the monosaccharide, wherein acid catalyst transforms monosaccharide into furfural, and subsequently with ring opening hydrogenation by the metal catalyst in molecular hydrogen [9]. Noting that the dehydration of monosaccharide or corncob to furfural is a commercial process, many efforts are devoted to the aqueous phase hydrogenolysis of biomass-derived furfural and furfural alcohol with platinum, ruthenium or non-precious copper catalyst [8, 10-12]. The ring-opening process to 1,2-PeD is well understood with reaching a high 1,2-PeD yield (about 73%) [5]. However, the key deficiencies of this multistep strategy lie in high operating, purification cost and quite inefficient dehydration process, achieving only ~50% of the theoretical furfural yield owing to

the degradation and polymerization reactions of furfural, thus the overall 1,2-PeD yield could hardly exceed the furfural yield in the multistep process.

More recently, an efficient one-pot conversion strategy without isolation of the platform intermediates has been extensively studied for optimizing the technology and route [13-15][16, 17]. Nijhuis et al. uncover one-pot synthesis of 1,2-PeD and 1,4-PeD with xylose dehydration coupled with hydrogenation process in the biphasic system [18], but the strategy has not been deeply explored and the obtained 1,2-PeD selectivity (< 10%) has yet to be improved. Looking into the major routes for the transformation of xylose in the coexistence of acid and hydrogenation catalysts, several types of reactions, namely, dehydration, hydrogenation, hydrogenolysis, degradation and polymerization reactions were mainly involved [19]. These reactions interplay with each other, making the product distribution of the whole reaction, from sugar alcohol and diols to furanic compounds, strongly depend on the rate matching among them. Hence, the product selectivity control is an important and significative issue in this complicated system.

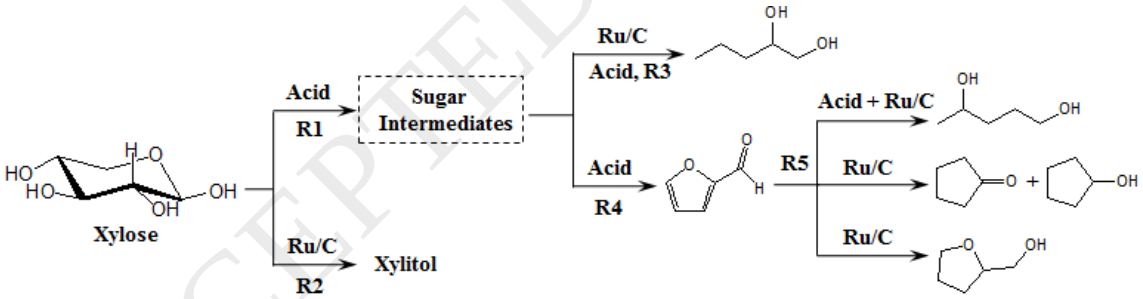

Scheme 1 Reaction network for one-pot conversion of xylose in acid-metal dual catalyst system

According to our previous work [20], a reaction network for one-pot conversion of xylose in the dual catalyst system is illustrated in scheme 1. When acid and hydrogenation catalysts are integrated into a single phase system, xylitol is the main product because of its thermodynamical benefit for xylose hydrogenation reaction. While the aqueous biphasic system can dramatically suppress xylose

hydrogenation and ensure xylose be converted into other hydrogenation products. Notably, 1,2-PeD is the main product among these products when ruthenium, an active metal for aqueous-hydrogenation of biomass-derived oxygenates to 1,2-PeD, is used as the metal catalyst [12, 21]. Herein, 1,2-PeD is targeted as an objective product for the product selectivity control in our catalyst system.

As previously mentioned, acid and hydrogenation catalysts are involved in the one-pot conversion of xylose, both can make a significant effect on product distribution. In order to simplify research, we firstly analyze the apparent activation energy of one-pot conversion process. The results indicate that the energy barrier for one-pot conversion process is from xylose dehydration reaction, suggesting that acid catalyst plays the primary role in tuning product distribution. Thus, acid catalysis dominated variation of product selectivity is emphatically investigated in the present contribution. Herein, Ru/C is used as a metal catalyst for all reactions.

When considering acid catalysts for monosaccharide dehydration, various materials including homogeneous and heterogeneous acids have been tested. Of these materials, niobium-based catalyst is an essential part because of its excellent water tolerance and unique acidic properties [22-28]. Furthermore, porous niobium phosphate with high activity and stability has been synthesized and tested [27, 29]. More importantly, the Lewis and Brønsted acid site densities are tunable by simply adjusting preparation conditions. Thus, niobium phosphates are introduced as acid catalysts in view of tunable acid site in this work. We use hydrothermal method to prepare a series of niobium phosphate solid acids with different surface Lewis/Brønsted ratio and address the effect of different acid site on the combined selectivity to 1,2-pentanediol and its precursor 1-hydroxyl-2-pentanone.

2. Experimental section

2.1. Materials and Catalysts. The following chemicals and solvents were used without further purification. Cyclohexane (AR), γ-valerolactone (98%), xylose (99%), xylitol (99%), furfural (98%), 1,2-pentanediol (98%), 1,4-pentanediol (98%), tetrahydrofurfuryl alcohol (98%), cyclopentanone (97%), cyclopentanol (99%), n-pentyl alcohol (99%), and sec-pentanol (99.5%) were purchased from Sigma-Aldrich. 1-Hydroxyl-2-pentanone was purchased from Zhejiang University of Technology. Niobium phosphate samples were synthesized by a hydrothermal method according to a literature method with slight modification [29]. Typically, 3.9 g of ammonium monohydric phosphate (98.5%) and 5.4 g ammonium oxalate niobium (19-20% Nb) were dissolved in 120 ml deionized water which was added to a three-neck flask. A 45 ml solution containing 3.0 g cetyl-trimethyl ammonium bromide (CTAB, 99.0%) was dropwise added with stirring in the above solution. The pH value of the final solution was respectively adjusted to 2, 5, 7 and 10 using phosphoric acid and ammonium hydroxide. The solution was maintained at room temperature for 1 h under stirring, then aged in a Teflon-lined autoclave for 24 h at 433 K. The resulting suspension was filtered and washed with 800 ml deionized water and subsequently dried at 373 K overnight. The product was then calcined by the furnace at 773 K for 5 h. The synthesized solid acids at pH value of 2, 5, 7 and 10 were respectively designated as follow: NbPO-2, NbPO-5, NbPO-7 and NbPO-10. The Nb_2O_5 sample purchased from Sigma-Aldrich was also used for comparative studies. In addition, 1.0 wt.% Ru/C catalyst was prepared by incipient wetness impregnation with ruthenium chloride (ShanXi KaiDa Chemical Engineering CO., LTD) on active carbon. After impregnation, the activation was carried out in tube furnace under flowing H_2 at 523 K for 5 h.

2.2. Catalytic Reaction. The conversion of xylose was performed in a 100 ml stirred autoclave. In a typical experiment, 200 mg reagent, 200 mg acid catalyst, 50 mg hydrogenation catalyst, and 32 g

solvent were loaded into the vessel, respectively. The aqueous phase and organic solvent were used in the mass ratio of 1:1. After sealed and pressurized with H_2 to 3.0 Mpa, the reactor was heated to 423 K and stirred for 4 h, then the autoclave was cooled in an ice-water bath. Products were filtered through a membrane filter (0.2 μm pore size) prior to analysis. Xylose and xylitol were analyzed on an Agilent 1200 Series HPLC equipped with a refractive index detector with a Bio-Rad HPX-87H column using an aqueous solution of H_2SO_4 at 5 mmol/L as mobile phase (0.7 ml/min). 1,2-PeD and other products (1,4-PeD, CPO, CPL, FF, 1-H-2-P, THFA, GVL, n-pentyl alcohol, and sec-pentanol) were quantified by FID-GC (Shimadzu 2014C with a column of DB-FFAP, 30 m). The conversion of xylose, the selectivity and yield of products were determined from Eq. (1), Eqs. (2), and Eqs. (3), respectively.

$$\text{Conversion} = \frac{[\text{xylose}]_i - [\text{xylose}]_f}{[\text{xylose}]_i} \times 100\% \quad (1)$$

$$\text{Selectivity} = \frac{[\text{product}]}{[\text{xylose}]_i - [\text{xylose}]_f} \times 100\% \quad (2)$$

$$\text{Yield} = \frac{[\text{product}]}{[\text{xylose}]_i} \times 100\% \quad (3)$$

Where $[xylose]_i$ and $[xylose]_f$ represented the initial and final molar quantity of xylose, respectively. [product] represented the molar quantity of detected products by GC and HPLC. The reproducibility of the one-pot conversion process was tested using NbPO-10 as acid catalyst. Two repetitions were carried out and the results were shown in Table 2.

2.3. Isotope-Labeling Experiment. The experimental procedures were similar to that of common reactions. Typically, 200 mg of xylose was dissolved in 16 g of D_2O and 16 g of cyclohexane, then the Bruker Avance 600-MHz Spectrometer was used to determine the incorporation of D atoms in the produced furfural. The D content of each carbon was calculated from the added and measured band areas of furfural, which was normalized by dimethyl sulfone.

2.4 Catalyst Characterization. The N_2 adsorption-desorption isotherms of the samples were determined by the ASAP-2020 analyzer at liquid nitrogen temperature. The surface area, pore volume and average pore size were respectively calculated using the Brunauer–Emmett–Teller (BET) and Barrett-Joyner-Halenda (BJH) methods. X-ray diffraction (XRD) analysis was performed on a Bruker D8 advance instrument using Cu Kα with 0.03°(2θ) steps over 10-80°. The morphologies of the as-prepared samples were measured by a field emission Hitachi S-4800 scanning electron microscope (SEM). The Fourier transform infrared (FT-IR) absorption spectra were recorded on a NICOLET 6700 spectrometer, with 32 scans at an effective resolution of 4 cm^{-1}.

Temperature programmed desorption of ammonia (NH_3-TPD) was analyzed on a Micromeritics AutoChem II 2920 equipped with a thermal conductivity detector. For each experiment, the samples (100 mg) were pretreated at 573 K at 10 K/min for 1 h and cooled to 313 K in Ar gas atmosphere (30 ml/min) before exposed to NH_3 (10% NH_3/Ar, 30 ml/min) until surface saturation. The weakly adsorbed NH_3 was removed by flushing Ar (30 ml/min) for 0.5 h. After the baseline became stable, then desorption was programmed at 1073 K at 10 K/min.

Infrared spectra of pyridine adsorption (Py-IR) were recorded to determine the type and ratio of acid sites with NICOLET 6700 spectrometer. The samples were pressed into thin self-supported wafers, then placed in a sample cell coupled to a glass-circulation system. The samples were dehydrated in situ at 673 K for 1 h under vacuum (1×10^{-3} Pa). After the temperature was cooled down to 313 K, the spectrum was recorded as the background. Then pyridine molecules were adsorbed, the spectra presented were recorded after the excess pyridine was desorbed under vacuum for 1 h.

The X-ray photoelectron spectroscopy (XPS) spectra were acquired with a Thermo Escalab 250XI spectrometer with AlKα (1486.6 eV) as the X-ray source. Analysis chamber pressure was less

than 5×10^{-9} Torr. The energy step sizes of 0.1 eV were chosen for survey spectra. All binding energies scale was calibrated using the C 1s peak of adventitious carbon on the analyzed sample surface at 284.8 eV as the reference according. Surface atomic concentrations were calculated by integrating the area under the curve after subtraction of the background.

3. Results and discussion

3.1 Characterization of catalysts

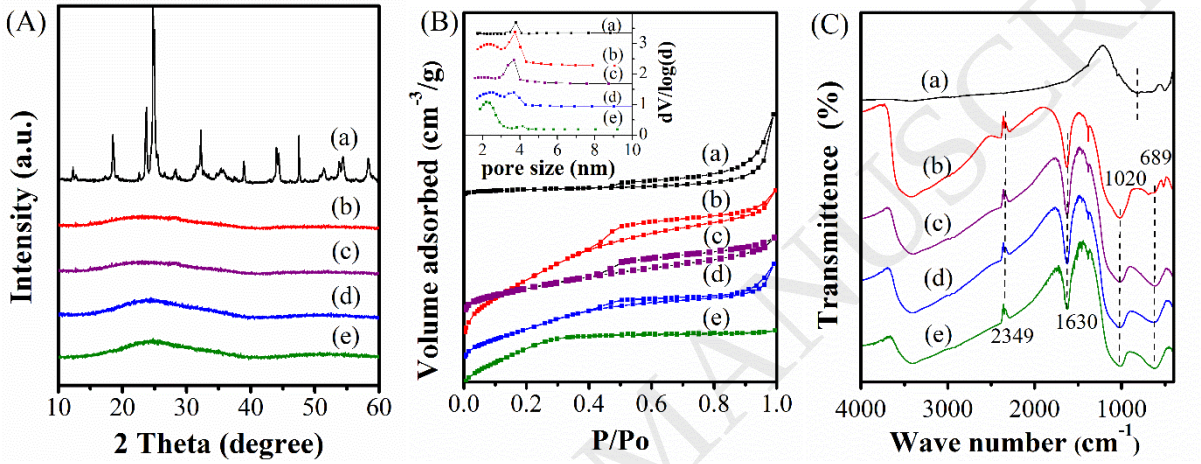

Fig. 1. XRD (A), N_2 adsorption-desorption isotherms (B) and FT-IR (C) patterns of (a) Nb_2O_5, (b) NbPO-2, (c) NbPO-5, (d) NbPO-7, (e) NbPO-10.

All the samples except Nb_2O_5 had similar XRD patterns, as shown in Fig. 1A. Nb_2O_5 was used as a reference catalyst due to its high Lewis acidity, which would be illustrated in detail below. The characteristic peaks of Nb_2O_5 at 2θ between 10°-60° were assigned to the monoclinic niobium oxide without peaks belonging to other phases according to the corresponding JCPDS card (PDF 27-1311). The NbPO samples in this study were confirmed to be amorphous by the presence of broad diffraction peaks, which was in accordance with the previous work [30]. The characterization by N_2 adsorption and EDS (Energy Dispersive Spectrometer) analysis to detect texture properties were shown in Fig. 1B and Table 1. A decrease in BET surface area, pore diameter and pore volume were observed when pH value varied from 2 to 10. In addition, as revealed by the bulk composition in

Table 1, a higher ratio of niobium to phosphorus was achieved for the final calcined products at higher pH value despite the same ratio of niobium to phosphorus was controlled in the precursor solution. It was reported that the niobium was assembled together to form precipitation instead of interacting with surfactant at higher pH value, thus leading to the decrease in surface area, pore diameter and pore volume, which could be also revealed by SEM images [29]. As seen in Fig. 2, the morphology of the NbPO-2 and NbPO-5 samples was needle-like particles, but the NbPO-7 and NbPO-10 samples were several micrometer particles without special morphology.

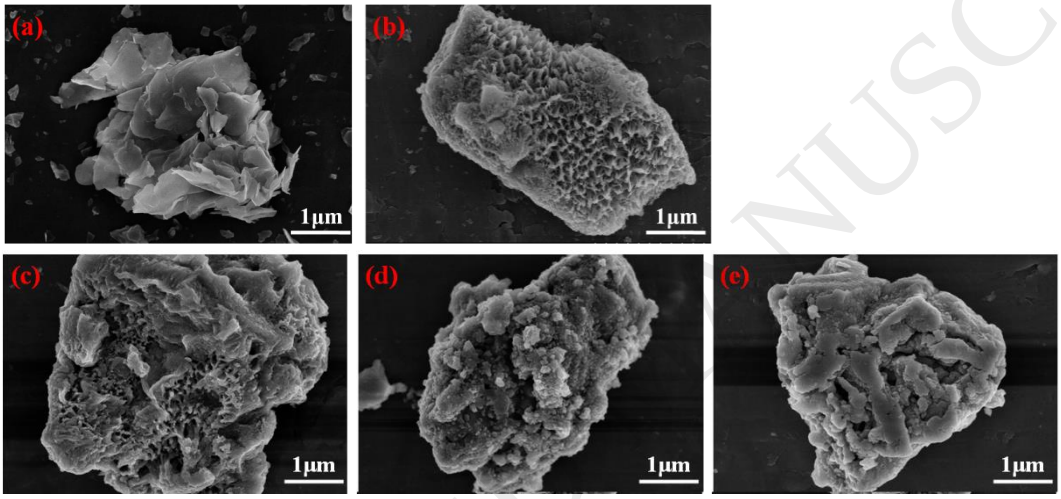

Fig. 2. SEM images of (a) Nb_2O_5, (b) NbPO-2, (c) NbPO-5, (d) NbPO-7, (e) NbPO-10.

The FT-IR spectra used for functional group characterization were shown in Fig. 1C. Peaks at 1020, 1630 and 2349 cm^{-1} could be clearly observed in all NbPO samples, but which were absent in Nb_2O_5. The bands at 2349 and 1630 cm^{-1} were assigned to the stretching and deforming vibrations of the (P)-OH group and the -OH group, respectively [31-33]. The bands at 1020 cm^{-1} corresponded to the stretching vibration of the Nb-O-P network [29], whereas the ratio of its peak area to that of Nb-O at 630 cm^{-1} was observed decreasing from NbPO-2 to NbPO-10. In addition, a broad adsorption centered around 689 cm^{-1} was found in the spectrum of Nb_2O_5 as well as NbPO samples due to the Nb-O stretching vibration mode. The phenomenon was associated with niobium and phosphorus contents detected by EDS analysis.

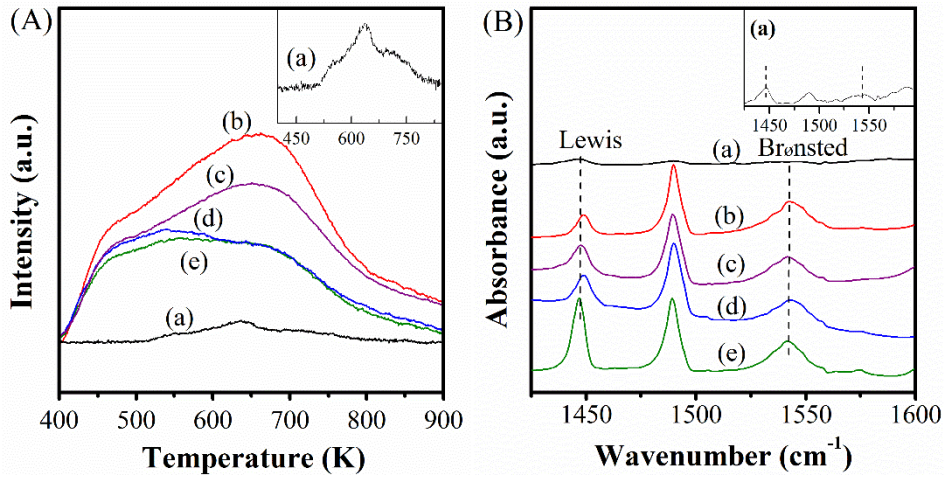

Fig. 3. NH_3-TPD spectra (A) and Py-IR spectra (B) on (a) Nb_2O_5, (b) NbPO-2, (c) NbPO-5, (d) NbPO-7, (e) NbPO-10.

The acid properties of the catalysts were studied by NH_3-TPD and Py-IR. Fig. 3A showed the results of NH_3-TPD experiments where all samples presented broad profiles in the range of 393-900 K, indicating the coexistence of weak, moderate and strong acid sites [33]. In addition, the acid properties were also quantificationally compared by NH_3 uptake and acid density (Table 1). Nb_2O_5 exhibited the lowest acidity, while the acid amount as well as strength of NbPO samples decreased from NbPO-2 to NbPO-10, as made evident by the significant changes in NH_3 uptake and the maximized desorption temperature. The Nb_2O_5 sample, seen in the inset of Fig. 3A, presented a broad peak between 523 K and 773 K due to the medium and strong solid acidity. As for NbPO samples, the medium strength acid sites in the range of 573-773 K, attributed to the terminal $P(OH)_2$ sites and surface P-OH sites [34], were much higher for NbPO-2 than those of NbPO-5, NbPO-7 and NbPO-10. It showed clearly that the acid properties of NbPO samples altered significantly with the change of pH value. To further explore this, the surface compositions of the catalysts were analyzed by XPS. Table 1 gave the surface concentration of niobium and phosphorus. Values given in the table exclude carbon and nitrogen [35]. The surface ratio of Nb/P was slightly lower than that of bulk ratio, indicating that surface depletion of niobium happened, however, the surface composition was still a function of the bulk composition. As reported, Nb_2O_5 has been receiving increasing interest as

solid Lewis acid catalyst for sugar dehydration due to its activity in water [36]. In addition, phosphorus could also act as Brønsted acid in the presence of OH groups. Thus the aforementioned change of surface composition could significantly affect the acidic species of NbPO samples. The individual concentrations of Brønsted and Lewis acid sites on NbPO samples were further quantified using Py-IR (Fig. 3B). The two absorption peaks located at 1445 and 1540 cm^{-1} were due to pyridine molecules interacting with the Lewis and Brønsted acid sites, respectively [37]. The areas of these two peaks were used to quantify the number of acid sites, and thus the ratios of Lewis to Brønsted acid site for NbPO samples were listed in Table 1. Obviously, the ratio of the Lewis to Brønsted acid site increased with the ratio of Nb/P, which can be attributed to the increase of surface niobium with high Lewis acidity (inset of Fig. 3B).

3.2 Optimization of reaction conditions

One-pot conversion of xylose under hydrogen pressure was carried out in the biphasic system to evaluate the effect of reaction condition. In order to avoid the difference induced by various batches of NbPO samples, the commercialized Nb_2O_5 was used as an acid catalyst for optimization experiments. Such a reaction in coexistence of acid and hydrogenation catalysts was rather complex since a multitude of compounds could be found, from sugar alcohol and diols to furanic compounds. Owing to thermodynamically beneficial to sugar hydrogenation, the hydrogenation of xylose to xylitol was preferred in the presence of hydrogenation catalyst. We have significantly suppressed the xylose hydrogenation in biphasic system using with the kinetic control strategy. Thus the dehydration of xylose, on the other hand, could occur over an acid catalyst and several sugar intermediates were generated. The sugar intermediate could not be captured due to its instability, but it was further dehydrated to produce furfural on acid sites or transformed to 1,2-PeD under the synergistic catalysis of acid and hydrogenation sites. In addition, the subsequent transformation of furfural could also obtain a variety of products such as 1,4-PeD, cyclopentanone (CPO), cyclopentanol (CPL),

tetrahydrofurfuryl alcohol and humins depending on the reaction pathway of C-C bond and C-O bond. For example, ring-opening hydrogenolysis yielded 1,4-PeD, the rearrangement of furan ring yielded CPO and CPL, the saturation of C=C bond yielded tetrahydrofurfuryl alcohol, and humins was formed by polymerization reaction. Therefore, the influence of reaction conditions on product distribution should be noteworthy in this complicated system.

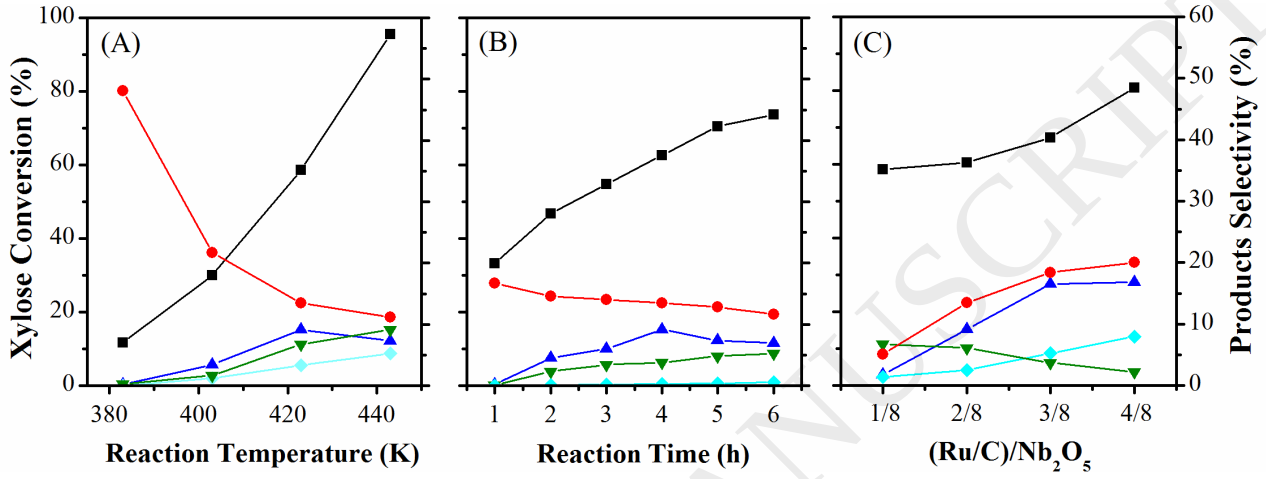

Fig. 4. One-pot conversion of xylose in biphasic system in function of reaction temperature (A), reaction time (B) and mass ratio of hydrogenation catalyst to acid catalyst (C). (■) xylose conversion; (●) selectivity of xylitol; (▲) selectivity of 1,2-PeD; (▼) the sum of CPO selectivity and CPL selectivity; (◆) selectivity of THFA; Reaction conditions: 3.0 Mpa of H_2 pressure, 4 h of reaction time, 0.2 g of xylose, 16.0 g of water, 16.0 g of cyclohexane, 0.2 g of Nb_2O_5.

As displayed in Fig. 4A, the conversion of xylose was only 11.7% with abundant xylitol while a little 1,2-PeD, 1,4-PeD, CPO and CPL being obtained at 383 K. With the increase of reaction temperature to 403 K, the conversion of xylose, selectivities of 1,2-PeD, CPO, CPL and THFA all increased along with significant decrease of xylitol selectivity. Further increased the reaction temperature, the 1,2-PeD selectivity increased first and then decreased, and the highest selectivity was obtained at 423 K. The 1,2-PeD selectivity passed through a maximum with time, implying the participation of 1,2-PeD in side reactions. However, the selectivities of 1,4-PeD, CPO and CPL

gradually increased with the increased temperature. The selectivity of xylitol changing in the opposite trend within the whole range of temperature indicated that the hydrogenation of sugar intermediates and furfural were kinetically favored over xylose reduction to xylitol when increasing reaction temperature.

In the Fig. 4B, the evolution of the conversion and product selectivity were shown as a function of reaction time. As expected, the xylose conversion increased with the increase of reaction time. The slight decrease of xylitol selectivity was observed probably because of the inactivation of hydrogenation catalyst or the involvement of other side reactions. More specifically, 5.6% yield of xylitol was obtained after only 1 h reaction and gradually reached the yield of 8.5% with the increase of reaction time to 6 h. 63.6% of xylitol was produced during the first one hour. This indicated that the hydrogenation of xylose occurred at the early stage of the reaction. In contrast, the selectivities of 1,2-PeD, THFA and CPO all increased continuously as a function of reaction time, but the highest 1,2-PeD selectivity was obtained after 4 h of reaction time. Further prolonged the time, 1,2-PeD would be converted to pentanol, thus decreasing the 1,2-PeD selectivity [9].

As the aforementioned reaction scheme, the various products except xylitol was generated by the subsequent hydrogenation of xylose dehydration products, each of these processes proceeding over both acid and hydrogenation catalysts. The adjustment of acid and hydrogenation sites in the dual catalyst system could tune the product distribution. Therefore, the impact on product selectivity with increasing mass of hydrogenation catalyst was investigated (Fig. 4C). A remarkable difference in the conversion of xylose, selectivity of xylitol, selectivity of 1,2-PeD and the selectivity of THFA was noticed, with selectivity varying up to 3-14 times. In the case of 1,2-PeD, the selectivity was 1.8% and obtained 24.3% when the hydrogenation catalyst was quadrupled. The results indicated the formation of hydrogenation products were meaningfully affected, rising with the concentration of hydrogenation sites in the reactor. Accordingly, the intensification of hydrogenation process was

accomplished by using γ-valerolactone-water/cyclohexane biphasic system [20]. A higher 1,2-PeD selectivity was obtained with almost no added hydrogenation catalyst. Hence, the optimized reaction conditions were obtained and γ-valerolactone-water/cyclohexane system was chosen in this work for further studies.

3.3 Catalytic performance of catalysts

Besides the remarkable differences in product selectivity induced by reaction conditions, the influence of acid catalyst was also proved to be noteworthy. Table 2 showed the results of xylose conversion achieved for different catalysts. The detected pentanol was not shown in Table 2 due to the small quantity (< 0.3%). Brønsted and Lewis acid catalysts were respectively used as an acid catalyst for one-pot conversion of xylose, the target product 1,2-PeD both appeared, which excluded the uniqueness of acid species for producing 1,2-PeD. Xylose was almost completely consumed (95.7%) after 4 h over phosphoric acid, while only 58.6% of xylose was converted due to the low acidity of Nb_2O_5, however, the selectivity of 1,2-PeD was slightly enhanced. In the case of NbPO-2 sample with high acidity, the catalytic activity was indeed improved and 1-hydroxyl-2-pentanone (1-H-2-P) appeared, which was considered as the precursor of 1,2-PeD. Subsequently, the catalytic behavior of NbPO-5, NbPO-7 and NbPO-10 catalysts was also evaluated in this system, the product selectivities were seen to be quite distinct. Before analyzing these results, we should remember well that xylitol was obtained from the direct hydrogenation of xylose; 1,2-PeD and 1-H-2-P were from the hydrogenation of sugar intermediates; 1,4-PeD, THFA, CPO and CPL were derived from the hydrogenation of produced furfural. Hence, xylose hydrogenation, sugar intermediate hydrogenation and furfural hydrogenation were the three main hydrogenation processes involved in the complicated one-pot conversion process. In order to illustrate the effect of acid catalyst on the product selectivity, the relationship between the product yield and the surface Lewis/Brønsted ratio were analyzed. As shown in Fig. 5, the product yields of sugar intermediate and furfural hydrogenation processes both

increased, while the product yield of xylose hydrogenation process decreased approximately linearly with the surface Lewis/Brønsted ratio, as will be discussed in detail below.

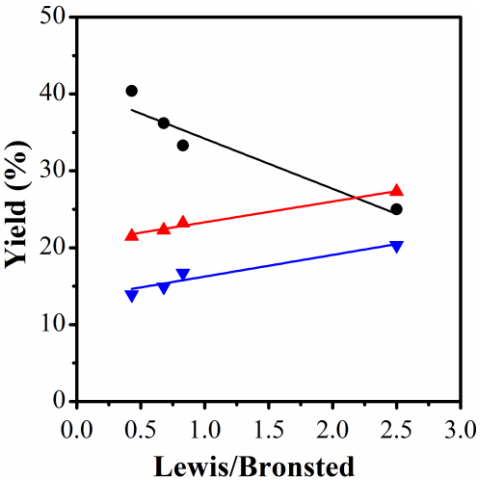

Fig. 5. Linear fitting of the product yield with the surface Lewis/Brønsted ratio; (●) xylose hydrogenation process, the yield of xylitol; (▲) sugar intermediate hydrogenation process, the total yield of 1,2-PeD and 1-H-2-P; (▼) furfural hydrogenation process, the total yield of 1,4-PeD, CPO, CPL and THFA.

3.4 Discussion

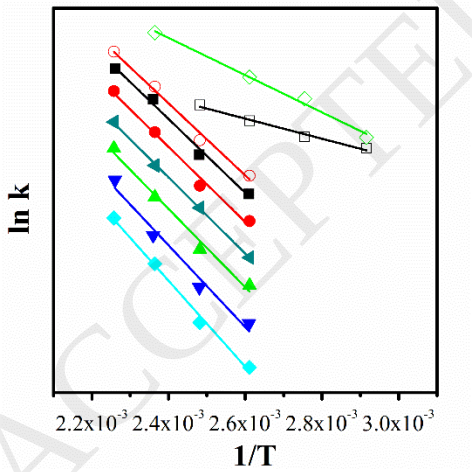

Fig. 6. Arrhenius plots for xylose conversion; (□) xylose hydrogenation over Ru/C in aqueous system; (○) xylose dehydration over Nb_2O_5 in aqueous system; (◊) xylose hydrogenation over Ru/C in water-cyclohexane biphasic system; (■) one-pot conversion over Nb_2O_5; (▼) one-pot conversion

over NbPO-2; (◀) one-pot conversion over NbPO-5; (▲) one-pot conversion over NbPO-7; (●) one-pot conversion over NbPO-10; (♦) one-pot conversion over H_3PO_4.

Extensive studies for biomass upgrading have been carried out by many groups to explore efficient transforming strategies such as retro-aldol condensation, C-O hydrogenolysis, and dehydration-hydrogenation reactions [18, 38, 39]. As for the conversion of xylose to 1,2-PeD, only the multistep dehydration-hydrogenation reactions with furfural as the reaction intermediate were achievable. More recently, an efficient one-pot conversion strategy in acid-metal dual catalyst system was developed. However, whether the process was multistep or one-pot, dehydration and hydrogenation reactions were the core steps in the network for xylose conversion. The assembly of these two type reactions was the challenge of obtaining high 1,2-PeD selectivity. As displayed in scheme 1, xylose could be hydrogenated to xylitol or dehydrated to sugar intermediates over Ru/C or H_3PO_4 catalysts. However, which was the preferred reaction in the coexistence of these two catalysts? The obtained apparent activation energies derived from the Arrhenius plots were respectively 13.2 KJ/mol and 56.7 KJ/mol for xylose hydrogenation and dehydration processes, revealing that xylose hydrogenation process was more thermodynamically beneficial. Furthermore, the result that 95.5 % selectivity of xylitol was obtained in aqueous system verified xylose hydrogenation being also dynamically beneficial. Therefore, the primary challenge to obtain 1,2-PeD was the xylose hydrogenation to xylitol, which was inert for the formation of 1,2-PeD in our system. In our previous work, the biphasic system showed distinct features in assembling dehydration and hydrogenation reactions, which was beneficial for the formation of 1,2-PeD. 34.6% yield of 1,2-PeD has been developed using kinetic control strategy [20]. The mass transfer resistance due to low xylose solubility of cyclohexane could significantly suppress xylose hydrogenation to xylitol, which was reflected in the apparent activation energy. As expected, the apparent activation energy increased to 24.8 KJ/mol in water-cyclohexane system. The results suggested that suppressing xylose hydrogenation reaction

could promote xylose being converted via dehydration process, thus improving the selectivity of 1,2-PeD.

After analyzing the advantage of biphasic system for assembling dehydration and hydrogenation reactions, we emphasized considering the impact of acid catalyst in dual catalytic system and gave an outlook for the product distribution. To explore this challenge, a first-order reaction rate expression to the biphasic xylose conversion kinetics was also fitted, the apparent activation energy was estimated to be 47.6 KJ/mol, considerably higher than those of xylose hydrogenation in aqueous and biphasic systems, but approaching to that of the xylose dehydration process (49.4 KJ/mol). Since the reaction mechanism of one-pot conversion of xylose to 1,2-PeD was not well understood, it remains a challenge to explain the observed differences in the apparent activation energy. However, in view of apparent activation energy, such results clearly indicated that the energy barrier for one-pot conversion process was from xylose dehydration reaction. This assumption agreed well with the observed remarkable difference in product selectivity induced by acid catalyst shown in Table 2 and Fig. 5. Hence, the catalytic ability of acid catalyst was the notable factor to adjust the product distribution. According to the aforementioned results, the NbPO samples were equipped with different amount of surface Lewis and Brønsted sites, and the 1,2-PeD as well as other hydrogenation product yields all increased linearly with the surface Lewis/Brønsted ratio detected by Py-IR analysis. Recently, Lewis acid has been determined as a more active and selective catalyst than homogeneous Brønsted catalysts [40]. For example, a cascade of reactions for xylose dehydration using Lewis catalyst plus Brønsted catalyst was more efficient [41], probably ascribed to the lower activation energy due to the difference in reaction mechanism [40]. However, caution was required for associating the catalytic performance with the acid properties characterized by Py-IR technology when considering the evolution of active site under reactive environment. Many Lewis acid sites of inorganic oxides were generally regarded as inactive sites for reactions in water, due to the formation of Lewis-base adducts by the coordination of water to the Lewis acid sites [36].

Although NbO_4 tetrahedra of niobium oxide could function as Lewis acid sites in water, a part of surface OH groups which acted as Brønsted acid sites were generated in these distorted polyhedrons [36]. These transformations eventually affected the contribution of acid sites in water.

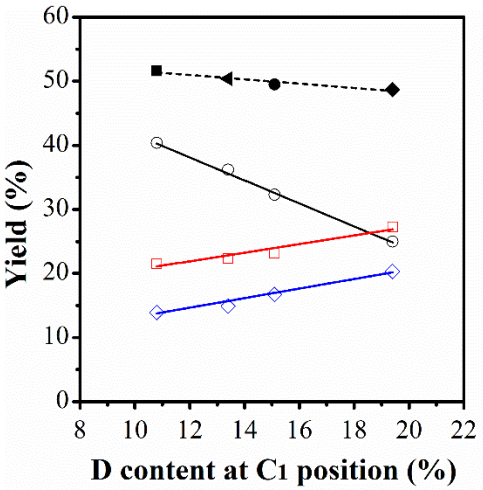

Fig. 7. Linear fitting of the product yield with the content of H/D exchange at C_1 position; (○) xylose hydrogenation process, the yield of xylitol; (□) sugar intermediate hydrogenation process, the total yield of 1,2-PeD and 1-H-2-P; (◊) furfural hydrogenation process, the total yield of 1,4-PeD, CPO, CPL and THFA;(■) the apparent activation energy over NbPO-2; (◄) the apparent activation energy over NbPO-5; (●) the apparent activation energy over NbPO-7; (♦) the apparent activation energy over NbPO-10.

To further clarify the practical impact of Lewis and Brønsted acid sites under reactive environment, the H/D exchange experiments in the cyclohexane-D_2O system were evaluated to demonstrate the contribution of different acid sites to xylose dehydration. According to dehydration mechanism shown in Table 3 (detailed mechanism could be found in reference [40, 42-44]), the H/D exchange at C_1 and C_3 positions of the resultant furfural could be used as an indicator for elucidation the contribution of Lewis and Brønsted acid sites for dehydration process. Notably, a content of 21.5% deuterium atom was observed only at the C_3 position over H_3PO_4, which coincided with the aldose-type mechanism over Brønsted acid. In the case of NbOP-2 sample with both Lewis and

Brønsted acid sites, furfural with 10.8% and 35.1% deuterium incorporation at C_1 and C_3 positions were respectively observed, where the H-D exchange at the C_1 position was catalyzed by Lewis acid site according to stepwise dehydration mechanism. It appeared that both Lewis and Brønsted acid sites were involved in H-D exchange at the C_3 position, and only Lewis acid site was involved at the C_1 position. Hence, the H-D exchange at the C_1 position could illustrate the contribution of Lewis acid site. Table 3 displayed the content of deuterium at the C_1 position for all NbPO samples. The results revealed that the contribution of Lewis acid site for xylose dehydration agreed well with the acid properties detected by Py-IR. Then the correlation between the product yield and the content of H/D exchange at the C_1 position was also analyzed (Fig. 7). Three inverse linear correlations were observed, revealing that Lewis acidity favored the high selectivities to sugar intermediate and furfural hydrogenation derived products such as 1,2-pentanediol, 1-hydroxyl-2-pentanone, 1,4-pentanediol, tetrahydrofurfuryl alcohol, cyclopentanone and cyclopentanol. Furthermore, the apparent activation energies of one-pot conversion over these catalysts were compared (see Table 2 and Fig. 7), it could be found that the apparent activation energies decreased with the increase of Lewis/Brønsted ratio. Hence, the advantage of Lewis acid site was reducing the activation energy of xylose dehydration, thus improving the selectivity of 1,2-PeD and its precursor.

4. Conclusions

The conversion of xylose in a one-pot process by using Ru/C and niobium phosphate dual catalyst system was shown. We have prepared and characterized a series of niobium phosphate catalysts with different surface Lewis and Brønsted acid sites and emphatically tested their effect on product distribution. Bulk and surface composition detected by EDS and XPS analysis revealed a higher niobium content for the niobium phosphate prepared at higher pH value, thus increasing the

ratio of surface Lewis to Brønsted acid site. When the ratio reaches 2.5, 14.0% selectivity of 1,2-pentanediol and 13.3% selectivity of 1-hydroxyl-2-pentanone were obtained at complete xylose conversion. We further demonstrated the contribution of Lewis and Brønsted acid sites to xylose dehydration under reactive environment using H-D exchange experiments, which agreed well with the acid properties obtained by NH_3-TPD and Py-IR technologies. Then the correlation between the product yield and the content of H/D exchange at the C_1 position was analyzed. The results revealed that catalysts with high Lewis acidity favored the high selectivities to 1,2-pentanediol and 1-hydroxyl-2-pentanone, but disfavored the selectivity to xylitol. This was due to the lower apparent activation energy of xylose dehydration reaction catalyzed by Lewis acid site.

Acknowledgements

This work was supported by the National Natural Science Foundation of China [grant No. 21676288]

References

[1] I.C. Agostini, S, USA 6296858, October 2, 2001.
[2] H.T. Nakamura, Y. , JP 201236121, February 23, 2012.
[3] P.G. CHEN G, ZENG T, CN 102584802-A, July 18, 2012.
[4] W. Y, CN 106397112-A, February 15, 2017.
[5] R. Ma, X.-P. Wu, T. Tong, Z.-J. Shao, Y. Wang, X. Liu, Q. Xia, X.-Q. Gong, ACS Catal., 7 (2017), pp. 333-337.
[6] G.R. Jenness, W. Wan, J.G. Chen, D.G. Vlachos, ACS Catal., 6 (2016), pp. 7002-7009.
[7] Y. Nakagawa, K. Tomishige, Catal. Today, 195 (2012), pp. 136-143.
[8] T. Mizugaki, T. Yamakawa, Y. Nagatsu, Z. Maeno, T. Mitsudome, K. Jitsukawa, K. Kaneda, ACS Sustain. Chem. Eng., 2 (2014), pp. 2243-2247.
[9] M. Chia, Y.J. Pagán-Torres, D. Hibbitts, Q. Tan, H.N. Pham, A.K. Datye, M. Neurock, R.J. Davis, J.A. Dumesic, J. Am. Chem. Soc., 133 (2011), pp. 12675-12689.
[10] H. Liu, Z. Huang, F. Zhao, F. Cui, X. Li, C. Xia, J. Chen, Catal. Sci. Technol., 6 (2016), pp. 668-671.
[11] T. Tong, Q. Xia, X. Liu, Y. Wang, Catal. Commun., 101 (2017), pp. 129-133.
[12] B. Zhang, Y. Zhu, G. Ding, H. Zheng, Y. Li, Green Chem., 14 (2012), pp. 3402.
[13] S. De, S. Dutta, B. Saha, ChemSusChem, 5 (2012), pp. 1826-1833.
[14] G.A. Kraus, T. Guney, Green Chem., 14 (2012), pp. 1593-1596.
[15] M.L. Ribeiro, U. Schuchardt, Catal. Commun., 4 (2003), pp. 83-86.
[16] S.J. Canhaci, R.F. Perez, L.E.P. Borges, M.A. Fraga, Appl. Catal. B-Environ., 207 (2017), pp. 279-285.
[17] R.F. Perez, M.A. Fraga, Green Chem., 16 (2014), pp. 3942-3950.
[18] V.V. Ordomsky, J.C. Schouten, J. van der Schaaf, T.A. Nijhuis, Appl. Catal. A-Gen., 451 (2013), pp. 6-13.
[19] M. Zheng, J. Pang, R. Sun, A. Wang, T. Zhang, ACS Catal., 7 (2017), pp. 1939-1954.
[20] N.L. Wang, Z.P. Chen, X.D. Mu, L.C. Liu, ChemSusChem, (2018).
[21] J. Lee, Y. Xu, G.W. Huber, Appl. Catal. B-Environ., 140–141 (2013), pp. 98-107.
[22] M.T. Reche, A. Osatiashtiani, L.J. Durndell, M.A. Isaacs, A. Silva, A.F. Lee, K. Wilson, Catal. Sci. Technol., 6 (2016), pp. 7334-7341.
[23] Y. Shao, Q. Xia, L. Dong, X. Liu, X. Han, S.F. Parker, Y. Cheng, L.L. Daemen, A.J. Ramirez-Cuesta, S. Yang, Y. Wang, Nat. Commun., 8 (2017), pp. 16104.
[24] G.S. Foo, D. Wei, D.S. Sholl, C. Sievers, ACS Catal., 4 (2014), pp. 3180-3192.
[25] C. García-Sancho, I. Agirrezabal-Telleria, M.B. Güemez, P. Maireles-Torres, Appl. Catal. B-Environ., 152-153 (2014), pp. 1-10.
[26] K. Tanabe, Catal. Today, 78 (2003), pp. 65-77.
[27] B. Pholjaroen, N. Li, Z. Wang, A. Wang, T. Zhang, J Energy Chem., 22 (2013), pp. 826-832.
[28] K. Tanabe, S. Okazaki, Appl. Catal. A-Gen., 133 (1995), pp. 191-218.
[29] Y. Zhang, J. Wang, J. Ren, X. Liu, X. Li, Y. Xia, G. Lu, Y. Wang, Catal. Sci. Technol., 2 (2012), pp. 2485-2491.
[30] R. Weingarten, Y.T. Kim, G.A. Tompsett, A. Fernández, K.S. Han, E.W. Hagaman, W.C. Conner, J.A. Dumesic, G.W. Huber, J. Catal., 304 (2013), pp. 123-134.
[31] D. Yu, J. Qian, N. Xue, D. Zhang, C. Wang, X. Guo, W. Ding, Y. Chen, Langmuir, 23 (2007), pp. 382-386.
[32] D. Yu, C. Wu, Y. Kong, N. Xue, X. Guo, W. Ding, J. Phys. Chem. C., 111 (2007), pp. 14394-14399.

[33] F. Li, L.J. France, Z. Cai, Y. Li, S. Liu, H. Lou, J. Long, X. Li, Appl. Catal. B-Environ., 214 (2017), pp. 67-77.
[34] R. Weingarten, Y.T. Kim, G.A. Tompsett, A. Fernández, K.S. Han, E.W. Hagaman, W.C. Conner, J.A. Dumesic, G.W. Huber, J. Catal., 304 (2013), pp. 123-134.
[35] H.J.M. Bosman, A.P. Pijpers, A.W.M.A. Jaspers, J. Catal., 161 (1996), pp. 551-559.
[36] K. Nakajima, Y. Baba, R. Noma, M. Kitano, J. N. Kondo, S. Hayashi, M. Hara, J. Am. Chem. Soc., 133 (2011), pp. 4224-4227.
[37] F. Liu, T. Wang, Y. Zheng, J. Wang, J. Catal., 355 (2017), pp. 17-25.
[38] N. Ji, T. Zhang, M. Zheng, A. Wang, H. Wang, X. Wang, J.G. Chen, Angew. Chem. Int. Ed., 47 (2008), pp. 8510-8513.
[39] S. Liu, Y. Okuyama, M. Tamura, Y. Nakagawa, A. Imai, K. Tomishige, Green Chem., 18 (2016), pp. 165-175.
[40] N.K. Gupta, A. Fukuoka, K. Nakajima, ACS Catal., (2017), pp. 2430-2436.
[41] V. Choudhary, S.I. Sandler, D.G. Vlachos, ACS Catal., 2 (2012), pp. 2022-2028.
[42] M.J. Antal, T. Leesomboon, W.S. Mok, G.N. Richards, Carbohyd. Res., 217 (1991), pp. 71-85.
[43] T. Ahmad, L. Kenne, K. Olsson, O. Theander, Carbohyd. Res., 276 (1995), pp. 309-320.
[44] M.J. Antal, W.S.L. Mok, G.N. Richards, Carbohyd. Res., 199 (1990), pp. 91-109.

Tables:

Table 1. Summary of physicochemical properties of solid acid catalysts

Catalyst	SSA[a] (m^2/g)	Pore size (nm)	Pore volume (cm^3/g)	NH_3 uptakes (μmol)[b]	Acid density (μmol/m^2)	L/B[c]	Bulk composition[d]				Surface composition[e]		
							Nb	P	Nb/P		Nb	P	Nb/P
Nb_2O_5	35	13.8	0.14	6.2	2.4	--	--	--	--		20.8	--	--
NbPO-2	427	3.7	0.40	473.6	11.0	0.4	10.9	13.7	0.8		7.4	14.9	0.5
NbPO-5	336	3.5	0.29	315.7	9.4	0.7	11.9	12.1	1.0		8.6	12.4	0.7
NbPO-7	267	3.4	0.20	234.1	8.8	0.8	13.5	9.2	1.5		11.8	10.6	1.1
NbPO-10	226	2.4	0.14	225.5	9.9	2.5	14.1	7.4	1.9		12.3	9.3	1.3

a: specific surface area; b; detected by NH_3-TPD; c: detected by Py-IR; d: detected by EDS analysis; e: detected by XPS analysis

Table 2. Catalytic results of one-pot conversion of xylose in aqueous biphasic system[a]

Acid	W/O[b]	Con. (%)	Sel[c]. (%)						Mass Balance (%)	Ea[d] (KJ/mol)
			Xylitol	1,2-PeD	1,4-PeD	1-H-2-P	THFA	CPO+CPL		
H_3PO_4	W/Cyclo	95.7	0.3	2.9	1.6	0.0	15.6	5.5	29.1	53.9
Nb_2O_5	W/Cyclo	58.6	13.5	9.1	0.0	0.0	3.3	6.7	60.5	47.6
Nb_2O_5	W-GVL/Cyclo	100.0	70.6	6.5	2.3	0.0	2.1	1.0	82.7	--
NbPO-2	W-GVL/Cyclo	100.0	40.4	16.7	4.7	4.8	7.9	1.3	75.9	51.6
NbPO-5	W-GVL/Cyclo	100.0	36.2	17.5	5.1	4.8	8.6	1.2	73.4	50.5
NbPO-7	W-GVL/Cyclo	100.0	32.2	19.1	6.5	4.1	8.8	1.4	72.2	49.5
NbPO-10	W-GVL/Cyclo	100.0	25.0	14.0	9.1	13.3	9.2	2.0	72.8	48.7
NbPO-10[e]	W-GVL/Cyclo	100.0	26.0	15.1	8.3	12.0	10.8	1.0	73.3	--
NbPO-10[f]	W-GVL/Cyclo	100.0	27.2	13.5	10.4	11.8	8.1	1.3	72.4	--

a: Reaction conditions: 0.2 g of xylose; 1.5 mmol H_3PO_4; 200 mg of solid acid catalyst; 50 mg of Ru/C catalyst; T = 423 K; t = 4 h; H_2 pressure: 3.0 Mpa; b: W represented aqueous phase; O represented organic phase; CYH and GVL were respectively abbreviation of cyclohexane and γ-valerolactone; 16 g of H_2O and 16 g of cyclohexane were added in W/CYH system; 4.8 g of H_2O, 11.2 g of γ-valerolactone and 16 g of cyclohexane were added in W-GVL/CYH system; c: 1,2-PeD: 1,2-pentanediol; 1,4-PeD: 1,4-pentanediol; FF: furfural; 1-H-2-P: 1-hydroxyl-2-pentanone; THFA: tetrahydrofurfuryl alcohol; CPO: cyclopentanone; CPL: cyclopentanol. d: apparent activation energy of one-pot conversion in water-cyclohexane biphasic system. e and f:: the one-pot conversion of two repetitions were used to indicate the degree of reproducibility.

Table 3. Catalytic results of xylose conversion in cyclohexane-D_2O system[a]

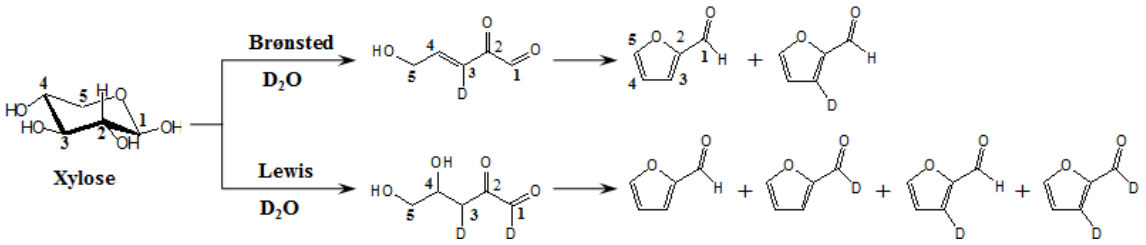

Cat	Con. (%)	FF[b] Sel. (%)	D content (%)	
			C_1	C_3
H_3PO_4	100.0	57.6	0.0	21.5
NbPO-2	99.8	57.1	10.8	35.1
NbPO-5	99.4	65.2	13.4	37.5
NbPO-7	91.5	70.5	15.1	40.6
NbPO-10	88.6	86.2	19.4	43.9
Nb_2O_5	43.4	47.4	27.2	50.9

a: Reaction conditions: 0.2 g of xylose; 1.5 mmol H_3PO_4; 200 mg of solid acid catalyst; T = 423 K; t = 4 h; N_2 pressure: 3.0 Mpa; 16 g of D_2O and 16 g of cyclohexane were added in W/CYH system; b: furfural.